ELSEVIER

Neurobiology of Aging 34 (2013) 128–136

NEUROBIOLOGY OF AGING

www.elsevier.com/locate/neuaging

Microglial activation in Alzheimer's disease: an (*R*)-[^{11}C]PK11195 positron emission tomography study

Alie Schuitemaker[a,b,*], Marc A. Kropholler[b], Ronald Boellaard[b], Wiesje M. van der Flier[a,c], Reina W. Kloet[b], Thalia F. van der Doef[b,e], Dirk L. Knol[c], Albert D. Windhorst[b], Gert Luurtsema[b], Frederik Barkhof[d], Cees Jonker[a], Adriaan A. Lammertsma[b], Philip Scheltens[a], Bart N.M. van Berckel[b]

[a] *Department of Neurology and Alzheimer Center, VU University Medical Center, Amsterdam, the Netherlands*
[b] *Department of Nuclear Medicine and PET Research, VU University Medical Center, Amsterdam, the Netherlands*
[c] *Department of Epidemiology and Biostatistics, VU University Medical Center, Amsterdam, the Netherlands*
[d] *Department of Radiology, VU University Medical Center, Amsterdam, the Netherlands*
[e] *Department of Psychiatry, University Medical Center Utrecht, Utrecht, the Netherlands*

Received 15 May 2011; received in revised form 6 April 2012; accepted 30 April 2012

Abstract

Inflammatory mechanisms, like microglial activation, could be involved in the pathogenesis of Alzheimer's disease (AD). (*R*)-[^{11}C]PK11195 (1-(2-chlorophenyl)-*N*-methyl-*N*-1(1-methylpropyl)-3-isoquinolinecarboxamide), a positron emission tomography (PET) ligand, can be used to quantify microglial activation *in vivo*. The purpose of this study was to assess whether increased (*R*)-[^{11}C]PK11195 binding is present in AD and mild cognitive impairment (MCI), currently also known as "prodromal AD."

Methods: Nineteen patients with probable AD, 10 patients with prodromal AD (MCI), and 21 healthy control subjects were analyzed. Parametric images of binding potential (BP_{ND}) of (*R*)-[^{11}C]PK11195 scans were generated using receptor parametric mapping (RPM) with supervised cluster analysis. Differences between subject groups were tested using mixed model analysis, and associations between BP_{ND} and cognition were evaluated using Pearson correlation coefficients.

Results: Voxel-wise statistical parametric mapping (SPM) analysis showed small clusters of significantly increased (*R*)-[^{11}C]PK11195 BP_{ND} in occipital lobe in AD dementia patients compared with healthy control subjects. Regions of interest (ROI)-based analyses showed no differences, with large overlap between groups. There were no differences in (*R*)-[^{11}C]PK11195 BP_{ND} between clinically stable prodromal AD patients and those who progressed to dementia, and BP_{ND} did not correlate with cognitive function.

Conclusion: Microglial activation is a subtle phenomenon occurring in AD.

Keywords: Alzheimer's disease; Mild cognitive impairment; Microglial activation; PET

1. Introduction

Alzheimer's disease (AD) is a neurodegenerative disorder, clinically characterized by progressive cognitive decline and impaired execution of daily activities (McKhann et al., 1984). Patients with mild cognitive impairment (MCI) have documented memory impairment but are still able to perform daily activities in a normal manner. MCI is considered to be a transitional phase between normal aging and AD (Petersen et al., 1999). Subjects with MCI have an increased risk of developing clinical AD of about 12% per year compared with 1%–2% in the general population (Petersen, 2004). Recently, new criteria for the diagnosis of AD were proposed, which allows diagnosis related to neuropathological changes in AD, based on the use of biomarkers

* Corresponding author at: Department of Neurology, Zuwe Hofpoort ziekenhuis, PO Box 8000, 3440 JD Woerden, the Netherlands. Tel.: +31 348 427911.
E-mail address: ASchuitemaker@zuwehofpoort.nl (A. Schuitemaker).

0197-4580
http://dx.doi.org/10.1016/j.neurobiolaging.2012.04.021

of AD (Dubois et al., 2010). According to this new classification, patients with MCI are considered to have "prodromal AD."

AD is characterized histopathologically by intracellular neurofibrillary tangles (NFT), extracellular deposits of amyloid in senile plaques, and diffuse loss of neurons (Braak and Braak, 1991). Although not a pathological hallmark specific to AD, activated microglia invariably are found in AD, and they may be present years before symptoms become apparent clinically (Petersen et al., 2006). Indeed, activated microglia could be an important therapeutic target, as microglial activation may be directly involved in the neurodegenerative process associated with AD (Yoshiyama et al., 2007).

Microglial activation can be quantified *in vivo* using positron emission tomography (PET) and (*R*)-[^{11}C]PK11195. (*R*)-[^{11}C]PK11195 (1-(2-chlorophenyl)-*N*-methyl-*N*-1(1-methylpropyl)-3-isoquinolinecarboxamide) is a highly specific ligand for the peripheral benzodiazepine-binding site (PBR). This site, also called the translocator protein (Papadopoulos et al., 2006), is expressed by cells of the mononuclear macrophage lineage and is markedly increased in activated microglia. Using (*R*)-[^{11}C]PK11195 and PET, microglial activation has already been demonstrated in several neurodegenerative diseases (Venneti et al., 2006). In AD, increased (*R*)-[^{11}C]PK11195 binding has been found in several brain areas (Cagnin et al., 2001; Yokokura et al., 2011). Recently, there have been two reports on (*R*)-[^{11}C]PK11195 binding in MCI (Okello et al., 2009; Wiley et al., 2009). In both studies, (*R*)-[^{11}C]PK11195 binding was assessed in two cohorts of MCI patients, being ^{11}C-labeled Pittsburgh compound B ([^{11}C]-PIB)-positive and -negative patients. These studies found either increased (Okello et al., 2009) or unchanged (Wiley et al., 2009) (*R*)-[^{11}C]PK11195 binding in MCI.

The purpose of the present study was to further investigate the extent and distribution of (*R*)-[^{11}C]PK11195 binding in larger cohorts of AD dementia and prodromal AD patients. A second aim was to establish whether presence of activated microglia in prodromal AD is associated with progression to AD dementia.

2. Methods

2.1. Subjects

Twenty patients with probable AD, 13 patients with MCI, and 21 healthy control subjects were included. Patients were recruited from the outpatient clinic of the Alzheimer center at the VU University Medical Center. All patients underwent standardized clinical assessment, including neurological and physical examinations, laboratory screening tests (including cerebrospinal fluid measures of amyloid β (Aβ), tau, and tau phosphorylated at threonine-181) (Bouwman et al., 2010), electroencephalogram (EEG), magnetic resonance imaging (MRI), and neuropsychological examination. Final diagnosis was established at a multidisciplinary consensus meeting. Diagnosis of probable AD was based on National Institute of Neurological and Communicative Disorders and Stroke-Alzheimer's Disease and Related Disorders Association (NINCDS-ADRDA) criteria (McKhann et al., 1984), and diagnosis of MCI on Petersen criteria (Petersen et al., 1999). Subjects underwent a standard battery of examinations, including history taking, medical and neurological examination, and neuropsychological examination, which consisted of the New York University Recall Test (NYU), Rey's Auditory Verbal Learning Test (RAVLT), Trail Making Test A and B, Fluency, Rey's complex figure, Boston Naming Test, and forward and backward condition of the Digit Span.

According to recently proposed criteria for prodromal AD (Dubois et al., 2010), MCI and AD patients were excluded from the analysis if there was no medial temporal lobe atrophy (MTA) or no abnormal cerebrospinal fluid profile (Bouwman et al., 2010) (one MCI patient). Consequently, MCI will be reported as prodromal AD. For clinical follow-up, prodromal AD patients visited the memory clinic annually. One patient progressed to dementia with Lewy bodies and was excluded from the analyses.

Control subjects without cognitive complaints were recruited by advertisement in local newspapers. All control subjects underwent the same diagnostic procedure (except EEG and lumbar puncture). Control subjects had to have age-corrected normal scores on neuropsychological assessments and a normal MRI (including MTA scores) (Bouwman et al., 2010), which was evaluated by a neuroradiologist.

Exclusion criteria for all subjects were known major psychiatric illness, previous head trauma with loss of consciousness of more than 1-hour duration, any significant metabolic disorder, and alcohol or substance abuse according to the Diagnostic and Statistical Manual of Mental Disorders-IV (DSM-IV) criteria (American Psychiatric Association, 2000). Intake of benzodiazepines, antipsychotic drugs, and non-steroidal anti-inflammatory drugs was not allowed because of possible interaction with (*R*)-[^{11}C]PK11195 binding. Written informed consent was obtained from all participants and in case of patients with AD also from a next of kin. The study protocol was approved by the Medical Ethics Review Committee of the VU University Medical Center.

2.2. MRI

All subjects had a structural MRI scan within 4 months of the PET procedure. MRI scans were acquired using a 1.0-T scanner (Magnetom IMPACT, Siemens Medical Solutions, Erlangen, Germany) and included a 3D heavily T1-weighted gradient echo sequence (magnetization prepared rapid acquisition gradient echo). Voxel size of the MRI images was $0.98 \times 0.98 \times 1.49$ mm^3. These scans

were used both for segmentation of gray and white matter and for delineation of regions of interest (ROI).

2.3. Production of (R)-[^{11}C]PK11195

(R)-[^{11}C]PK11195 was produced according to published methods (Shah et al., 1994). Each (*R*)-[^{11}C]PK11195 injection solution met the following pharmaceutical specifications: specific activity (SA) $>$ 18.5 GBq μmol^{-1}; radiochemical purity $>$ 98%; 5 $<$ pH $<$ 8.

2.4. PET

PET scans were acquired using an ECAT EXACT HR+ (Siemens/CTI, Knoxville, TN, USA) (Brix et al., 1997). First, a 10-minute transmission scan was performed in 2D acquisition mode using three retractable rotating line sources. This scan was used to correct the subsequent emission scan for photon attenuation. Then, a 3D dynamic (*R*)-[^{11}C]PK11195 emission scan was performed consisting of 22 frames with progressive increase in frame duration (1 $\times$ 30 background, 1 $\times$ 15, 1 $\times$ 5, 1 $\times$ 10, 2 $\times$ 15, 2 $\times$ 30, 3 $\times$ 60, 4 $\times$ 150, 5 $\times$ 300, and 2 $\times$ 600 seconds; total acquisition time 60.5 minutes). Detailed scanning procedures have been described previously (Mourik et al., 2010; Schuitemaker et al., 2007a, 2012). Subject motion during scanning was checked visually at regular intervals (by checking the position of the head using laser beams) and corrected immediately, if necessary.

2.5. Image reconstruction

All PET sinograms were corrected for dead time, tissue attenuation using the transmission scan, decay, scatter, and randoms. Data were reconstructed using a filtered back projection (FBP) reconstruction algorithm (Ollinger and Fessler, 1997), as well as a partial volume-corrected (PVC) ordered subset expectation maximization (OSEM) reconstruction algorithm that incorporates the scanner's point spread function in the system matrix during reconstruction. This PVC-OSEM algorithm has been validated previously. For PVC-OSEM, 4 iterations with 16 subsets and no loop or postfilter were used (Hudson and Larkin, 1994). Reconstructed images were filtered using a Hanning filter of 5 mm full width at half maximum (FWHM), both in transaxial and axial directions. A zoom factor of 2 and a matrix size of 256 $\times$ 256 $\times$ 63 were used, resulting in a voxel size of 1.2 $\times$ 1.2 $\times$ 2.4 mm^3 and a spatial resolution of approximately 2.5-mm full width at half maximum in the center of the field of view. Images were then transferred to workstations (Sun Microsystems, Santa Clara, CA, USA) for further analysis. One AD and one prodromal AD patient were excluded because of insufficient quality of the PET scans for regional analyses (movement artefacts).

2.6. Data analysis

Parametric images of binding potential (BP_{ND}) of (*R*)-[^{11}C]PK11195 were generated using receptor parametric mapping (RPM) (Gunn et al., 1997), a basis function implementation of the simplified reference tissue model (SRTM) (Lammertsma and Hume, 1996). RPM was found to be the most suitable parametric method for analysis of (*R*)-[^{11}C]PK11195 data (Schuitemaker et al., 2007a). Supervised cluster analysis was used to extract the reference tissue input curve directly from the dynamic (*R*)-[^{11}C]PK11195 data (Turkheimer et al., 2007). The primary outcome measure was BP_{ND} (Innis et al., 2007; Lammertsma and Hume, 1996).

2.7. Regions of interest definition

For each subject, PET and MRI scans were coregistered using the software package MIRIT (Maes et al., 1997; West et al., 1997). ROI were drawn manually on bilateral hippocampus, amygdala, entorhinal cortex, and lateral and superior temporal lobe using the software program DISPLAY, developed at the McConnell Brain Imaging Centre (BIC) of the Montreal Neurological Institute, McGill University (www.bic.mni.mcgill.ca/ServicesSoftwareVisualization/HomePage). ROIs were drawn manually by a trained researcher (A.S.) on the individual MRI scans in a plane by plane fashion according to anatomic structures. These 2D ROI can be defined in transaxial, coronal, and sagittal planes, and these orientations used for ROI definition could be changed anytime throughout the manual delineation process, thereby facilitating generations of 3D ROIs. In addition, template ROIs were defined using probability map-based automatic brain delineation (Svarer et al., 2005). ROIs in this template include the frontal cortex (volume-weighted average of superior frontal, orbital frontal, and medial inferior frontal cortex), cingulate posterior cortex, thalamus, parietal cortex, and occipital cortex. Regional values of BP_{ND} were obtained by projecting the manual and template ROIs, defined above, onto the parametric BP_{ND} images.

2.8. Statistical analysis

Statistical analyses of ROI data were performed using SPSS software (SPSS Institute, Chicago, IL, USA), version 15.0. Values are presented as mean $\pm$ standard deviation (SD). Differences in clinical characteristics, tracer doses, and specific activity between different subject groups were tested using analysis of covariance (ANCOVA) with post hoc Bonferroni corrections and age as a covariate. A linear mixed model was used to assess group differences in regional binding. Mixed models use all data available from all cortical regions, properly account for within-person correlations over the different cortical regions, and appropriately handle missing data. The model included diagnosis, region, and interaction of diagnosis and region. Age was used as a covariate, and BP_{ND} was the dependent variable. The threshold for significance was set at $p < 0.05$. Analyses were repeated with prodromal AD and AD combined as one patient group and compared with healthy control subjects. Associations between (*R*)-[^{11}C]PK11195 binding and cognitive test re-

sults were evaluated using Pearson correlation coefficient adjusted for multiple comparisons.

2.9. Voxel-wise analysis

Voxel-wise analysis of parametric BP_{ND} images was performed using statistical parametric mapping (SPM) (SPM2; www.fil.ion.ucl.ac.uk/spm). The purpose of this analysis was to assess whether there were clusters of voxels with altered binding that could not be identified in the ROI analysis, for example due to heterogeneity within and across ROIs. As voxel-wise analysis is very sensitive to patient movement, scans were checked visually for motion artefacts prior to SPM analysis. Standard additional smoothing within SPM using a 10-mm full width at half maximum Gaussian filter was performed to reduce noise to acceptable levels and to obtain sufficient overlap of structures between subjects for SPM analysis. Differences between AD dementia or prodromal AD patients (and subgroups of [non]converters) and healthy control subjects were assessed in a voxel-wise comparison, using two sample *t* tests. SPM analyses were performed without proportional scaling. Proportional scaling can be omitted because RPM plots are quantitatively accurate even at lower noise levels, as shown previously (Schuitemaker et al., 2007b). SPM results were thresholded at both $p < 0.01$ and $p < 0.001$. The false discovery rate method to correct for multiple comparisons within SPM was used to provide corrected *p*-values (Genovese et al., 2002).

3. Results

3.1. Demographic and clinical data

Baseline characteristics of participants, eligible for analysis, are presented in Table 1. There were no differences in age or gender between AD patients, prodromal AD patients, and healthy control subjects. MTA score was lower in healthy control subjects compared with prodromal AD or AD dementia patients. AD dementia patients had lower Mini-Mental State Examination (MMSE) scores (Folstein et al., 1975) than healthy control subjects and prodromal AD patients, and scores in prodromal AD patients were lower than those in healthy control subjects. AD dementia patients and prodromal AD patients had lower scores on the NYU paragraph recall test, the RAVLT, and the backwards condition of the digit span compared with control subjects. AD dementia patients had higher scores on the trail making test A compared with control subjects and prodromal AD, and on the trail making test B compared with control subjects. Seven of the 10 prodromal AD patients progressed clinically and fulfilled AD dementia criteria at follow-up. Three patients remained clinically stable until they were lost to follow up (mean follow-up duration was 2.7 ± 0.5 years; range, 2.3–3.3 years). Mean duration of follow-up for patients until converting to dementia was 2.6 years (SD = 1.6; range, 1.1–5.8 years). Prodromal AD patients who converted to AD dementia had higher scores on the forward condition of the digit span than patients who did not convert (6.3 vs. 4.7; $p = 0.011$). Otherwise, there were no differences in cognitive test results at baseline between converters and nonconverters ($p \geq 0.05$).

Table 1
Subject characteristics

	Controls	Prodromal AD	AD
N	21	10	19
Age (years)	68 ± 8	72 ± 6	69 ± 8
Sex M : F	13 : 8	7 : 3	11 : 8
MTA score	0.3 ± 0.4	1.3 ± 0.6	1.5 ± 0.9
MMSE[a,b,c]	29 ± 1	26 ± 1	23 ± 3
NYU test score[a,b]	9.2 ± 4.2	3.9 ± 1.7	1.3 ± 1.9
RAVLT[a,b]	8.6 ± 3.2	2.1 ± 2.2	0.4 ± 0.7
Trail A[b,c]	43 ± 12	46 ± 14	71 ± 22
Trail B[b]	89 ± 34	139 ± 68	190 ± 87
Digit forward	6.4 ± 0.9	5.8 ± 1.0	6.1 ± 1.0
Digit backward[a,b]	5.7 ± 1.1	3.7 ± 0.5	4.5 ± 1.2

Data are represented as mean ± SD.
Key: AD, Alzheimer's disease; MTA score, mean medial temporal lobe atrophy; MMSE, Mini-Mental State Examination; NYU, New York University paragraph recall test; RAVLT, Rey's Auditory Verbal Learning Test; Trail A and B, trail making test A and B; Digit forward and backward, forward and backward condition of the digit span.
[a] $p < 0.05$ for controls vs. prodromal AD.
[b] $p < 0.05$ for controls vs. AD.
[c] $p < 0.05$ for prodromal AD vs. AD.

3.2. (R)-[^{11}C]PK11195 administration

There were no differences in injected tracer dose or specific activity between subject groups. Mean tracer dose was 350 ± 102, 295 ± 159, and 303 ± 87 MBq ($F(2,45) = 1.14$, $p = 0.33$), and mean specific activity was 79 ± 36, 84 ± 41, and 92 ± 35 Gbq·μmol^{-1} ($F(2,47) = 0.62$, $p = 0.54$) in AD dementia patients, prodromal AD patients, and healthy control subjects, respectively. Estimated receptor occupancy associated with these high SA tracer doses was <1%.

3.3. ROI analysis

In Table 2, RPM-derived BP_{ND} values of (*R*)-[^{11}C]PK11195 are shown for different brain regions in AD dementia patients, prodromal AD patients, and healthy control subjects, using the standard FBP reconstruction algorithm. Linear mixed models showed no significant main effect of diagnostic group ($p = 0.53$). There was an effect of brain region ($p < 0.001$). No interaction was found ($p = 0.11$), indicating that regional differences were similar across diagnostic groups. This is also illustrated in Fig. 1, showing BP values in the different subject groups. In general, BP_{ND} was highest in frontal lobe, posterior cingulate cortex, thalamus, parietal, and occipital lobes. Results were similar (main effect of brain region [$p < 0.001$], but no main effect of diagnostic group [$p = 0.93$] and no interaction [$p = 0.13$]) when images with higher spatial resolution, as obtained with the PVC-OSEM reconstruction algorithm, were used.

Table 2
Regional values of (*R*)-[^{11}C]PK11195 BP_{ND}

ROIs	Controls	Prodromal AD	AD
Frontal	0.182 ± 0.101	0.202 ± 0.128	0.231 ± 0.127
Cingulate posterior	0.370 ± 0.133	0.387 ± 0.142	0.338 ± 0.172
Lateral temporal	0.054 ± 0.094	0.067 ± 0.111	0.079 ± 0.108
Superior temporal	0.132 ± 0.141	0.136 ± 0.167	0.177 ± 0.092
Amygdala	−0.103 ± 0.171	−0.167 ± 0.193	−0.054 ± 0.167
Hippocampus	−0.049 ± 0.112	−0.032 ± 0.207	0.014 ± 0.120
Entorhinal	−0.156 ± 0.145	−0.080 ± 0.240	−0.047 ± 0.176
Thalamus	0.234 ± 0.090	0.279 ± 0.168	0.311 ± 0.182
Parietal	0.202 ± 0.124	0.234 ± 0.156	0.199 ± 0.134
Occipital	0.439 ± 0.108	0.462 ± 0.054	0.427 ± 0.144

Data are represented as mean ± SD.
Key: ROIs, regions of interest; AD, Alzheimer's disease.

When the analyses were repeated, with prodromal AD and AD dementia combined as one patient group, comparable results were obtained.

3.4. Voxel-wise analysis

Voxel-wise analysis of BP_{ND} images showed increased (*R*)-[^{11}C]PK11195 binding in AD dementia patients compared with healthy control subjects in bilateral occipital cortex ($p = 0.01$) (Fig. 2). At a higher statistical threshold ($p = 0.001$), no increased signal was found. No differences in (*R*)-[^{11}C]PK11195 binding between prodromal AD patients (and subgroups) and healthy control subjects or AD dementia patients were found. When the analyses were repeated with prodromal AD patients and AD dementia patients as one group and compared with healthy control subjects, no differences were found.

3.5. (R)-[^{11}C]PK11195 binding potential and cognition

There were no correlations with cognitive tests at baseline and (*R*)-[^{11}C]PK11195 BP_{ND} in any region. There was no difference in BP_{ND} between prodromal AD patients who remained clinically stable and those who progressed clinically to dementia.

4. Discussion

In this study, only small clusters of increased (*R*)-[^{11}C]PK11195 binding were found in bilateral occipital lobe in AD dementia patients using a voxel-based analysis. ROI-based analyses showed no differences between diagnostic groups, with large overlap between subject groups. This suggests that microglial activation in AD is a subtle phenomenon, which is present in AD dementia.

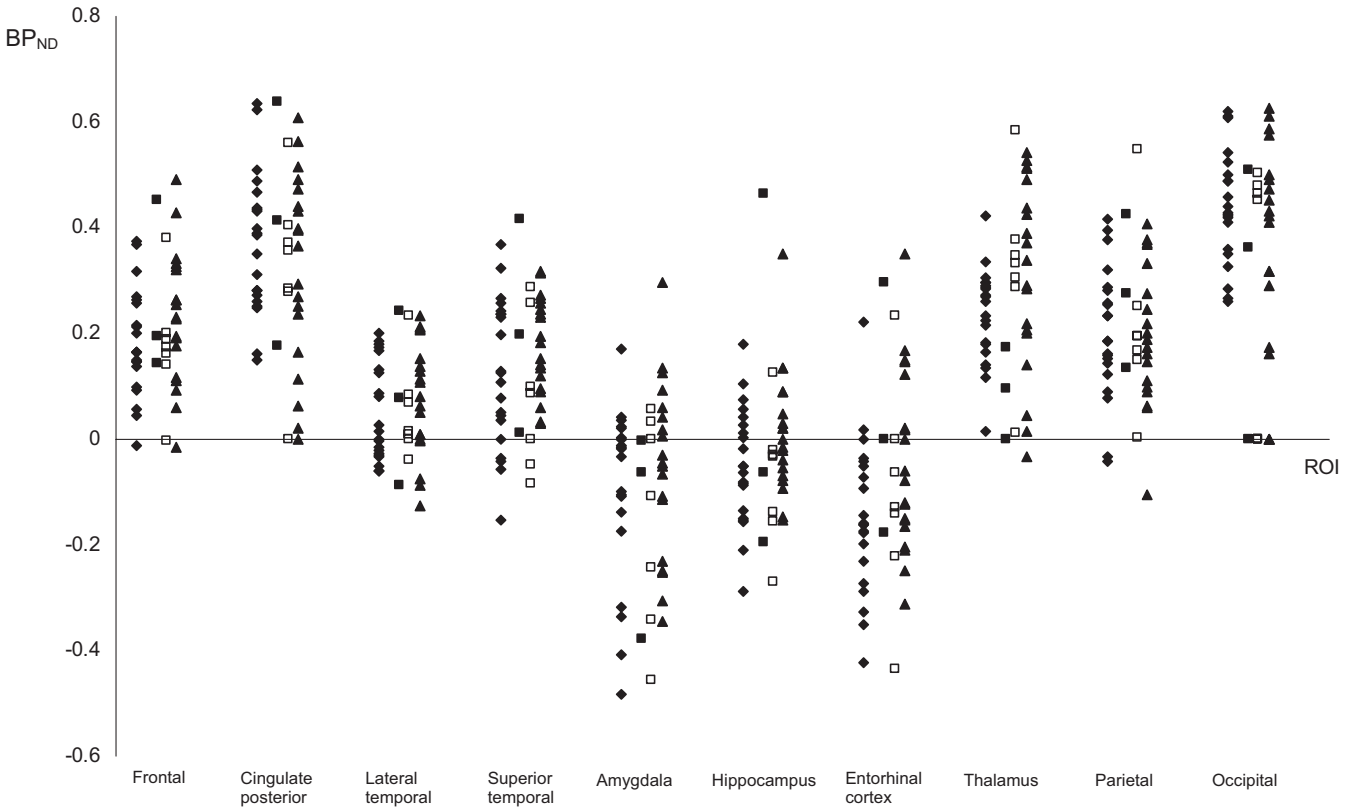

Fig. 1. (*R*)-[^{11}C]PK11195 BP_{ND} in healthy control subjects, prodromal Alzheimer's disease (AD), and AD dementia patients. ◆ = controls, ■ = patient with prodromal AD who remained clinically stable, □ = patients with prodromal AD who progressed to dementia, and ▲ = AD dementia patients.

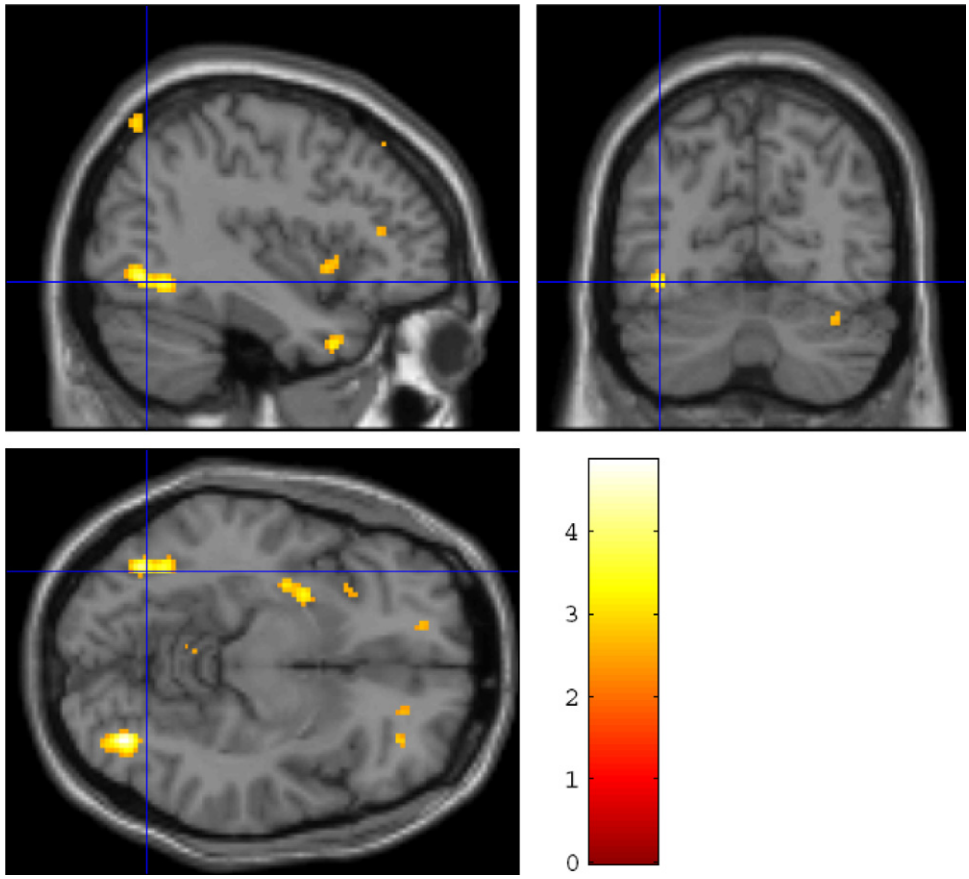

Fig. 2. Regions with increased (*R*)-[^{11}C]PK11195 BP_{ND} in Alzheimer's disease dementia compared with healthy control subjects. Images were thresholded at $p = 0.01$. Extent threshold = 10 voxels. The colour bar indicates *T* values. Data were corrected for multiple comparisons using the false discovery rate method within SPM. For interpretation of the references to color in this figure legend, the reader is referred to the Web version of this article.

Quantification of (*R*)-[^{11}C]PK11195-specific binding (BP_{ND}) was performed using RPM (Schuitemaker et al., 2007a) and a modified supervised cluster analysis (Boellaard et al., 2008; Turkheimer et al., 2007; Yaqub et al., 2009) to extract the reference tissue input curve. Given the relatively low specific signal in AD and especially prodromal AD, it is essential to use optimal methodology. For quantification, use of a pure enantiomer, in this case (*R*)-[^{11}C]PK11195, is mandatory (Shah et al., 1994). In addition, it has been shown that in pathological conditions like AD, with reduced flow rates or variations in blood volume, a basis function method is preferred above other simplified methods, such as standardized uptake values (Hoekstra et al., 2000) or (reference) Logan plot analysis (Logan et al., 1990, 1996), for analyzing (*R*)-[^{11}C]PK11195 data because it produces less bias and is more precise (Schuitemaker et al., 2007a). As such, RPM with an optimized supervised cluster analysis to extract the reference tissue curve was used in this study.

The present findings are largely in agreement with previous (*R*)-[^{11}C]PK11195 studies in AD, in which cluster (Cagnin et al., 2001) or supervised cluster analysis methods (Edison et al., 2008) were used to derive the reference region and in which also subtle increased (*R*)-[^{11}C]PK11195 binding was demonstrated. To date, two (*R*)-[^{11}C]PK11195 studies in MCI patients have been reported (Okello et al., 2009; Wiley et al., 2009). In both studies, (*R*)-[^{11}C]PK11195 binding was examined in [^{11}C]PIB-positive and -negative patients, where [^{11}C]PIB was used as a biomarker of disease severity. Wiley et al. (2009) reported (*R*)-[^{11}C]PK11195 binding in cerebellum, mesial temporal cortex, sensorimotor cortex, frontal cortex, parietal cortex, and posterior cingulate cortex but did not demonstrate significant differences between diagnostic groups, comparable with the present results. Okello et al. (2009) did demonstrate increased (*R*)-[^{11}C]PK11195 binding in the frontal cortex in a small group of [^{11}C]-PIB positive patients, although no correlations between amyloid depositions, as measured with [^{11}C]PIB, and (*R*)-[^{11}C]PK11195 binding in frontal cortex were found.

In the present study, only patients with the most common subtype of MCI, amnestic MCI, currently defined as prodromal AD (Dubois et al., 2010; Petersen et al., 1999), were included. Neuropathological data indicate that many amnestic MCI patients have already high numbers of plaques and tangles (Morris et al., 2001; Petersen et al., 2006; Price and Morris, 1999), especially in the medial temporal lobe (Petersen et al., 2006; Price and Morris, 1999), as has been

acknowledged in the new proposed criteria for AD, in which patients with biomarker-positive amnestic MCI are considered to have a predementia stage of AD (prodromal AD) (Dubois et al., 2010). This is in agreement with postmortem studies demonstrating that activation of microglia precedes neurodegenerative changes in the neocortex (Rozemuller et al., 1989; Veerhuis et al., 2003). Indeed, a gradual increase of microglial activation with increasing Braak scores of neurofibrillary changes and with Congo red-positive deposits has been reported (Arends et al., 2000; Hoozemans et al., 2005). As clinicopathological and animal studies have demonstrated that microglia are attracted to the site of amyloid plaque formation (Arends et al., 2000; Meyer-Luehmann et al., 2008), one could expect increased (*R*)-[^{11}C]PK11195 binding in regions with reported Aβ deposition. Consequently, one might expect increased (*R*)-[^{11}C]PK11195 binding in prodromal AD patients, who progress to AD dementia, but also even earlier in preclinical AD. In this context, regional increases in (R)-[^{11}C]PK11195 binding in prodromal AD might reflect early changes, associated with Aβ deposition, occurring before structural changes can be seen. However, no differences in (*R*)-[^{11}C]PK11195 binding were found between prodromal AD patients who stayed stable and those who progressed to dementia.

Moreover, although some trends were observed, none of the observed correlations between cognitive scores at baseline and (*R*)-[^{11}C]PK11195 BP_{ND} in any of the brain regions in prodromal AD or AD dementia patients were significant after correction for multiple statistical comparisons. Previously, Yokokura et al. (2011) examined (*R*)-[^{11}C]PK11195 binding as well as [^{11}C]-PIB and glucose metabolism in a relatively small group of AD patients and demonstrated a correlation between (*R*)-[^{11}C]PK11195 binding and MMSE scores in AD. Okello et al. (2009) also explored correlations between (*R*)-[^{11}C]PK11195 binding and cognition in a small group of MCI patients and reported no correlations between (*R*)-[^{11}C]PK11195 binding and MMSE in PIB-positive MCI patients, which is in agreement with the present results. Because the sample size was relatively small and the follow-up period relatively short, a larger study is needed to confirm these findings. Furthermore, to assess (*R*)-[^{11}C]PK11195 binding in the earliest stages of AD, it would also be interesting to study asymptomatic-at-risk or presymptomatic AD subjects (Dubois et al., 2010).

Remarkably, ROI-based analyses showed relatively low regional binding in the medial temporal lobe regions (Fig. 1). Relatively low BP_{ND} might be caused by partial volume effects, especially in relatively small regions surrounded by cerebrospinal fluid, such as hippocampus and entorhinal cortex, or by a relatively higher binding in the reference region than that in the target region. To limit partial volume effects, a novel PVC-OSEM reconstruction algorithm was also applied, but this did not affect results. An alternative explanation could be that within an ROI, a relatively smaller region shows increased (R)-[^{11}C]PK11195 binding. As such, averaging all voxels within a predefined ROI may dilute a potential signal in part of that ROI and could therefore lead to false-negative findings. This might also explain the differences between voxel-based and ROI-based methods, as voxel-based methods do not suffer from this "dilution" effect.

The present results, describing only small areas with increased (*R*)-[^{11}C]PK11195 binding, suggest that microglia activation in AD is a subtle phenomenon. An important question is whether microglial activation plays a harmful or beneficial role in the development of AD. The function of microglia in the brain is twofold. In normal brain tissue, they survey the brain environment and when structural or functional integrity of the brain is threatened they transform to activated states. When activated, microglia can have both neuroprotective and neurotoxic roles (Akiyama et al., 2000). As such, it is possible that activated microglia may induce neuronal damage. In AD, microglial activation occurs around neuritic plaques, where it may be involved in the degradation and phagocytosis of Aβ deposits (Akiyama et al., 2000). This could constitute a beneficial effect of microglia activation. Activated microglia, however, are also present in areas with low amyloid load, indicating that other mechanisms than plaque formation appear to contribute to microglial activation (DiPatre and Gelman, 1997). Indeed, in an animal model of AD, microglial activation and loss of synapses preceded tangle formation (Yoshiyama et al., 2007), suggesting that microglial activation and neuronal damage are closely connected. Although preclinical studies do not provide conclusive evidence for either a neuroprotective or neurotoxic role of activated microglia in AD, converging data indicate that "inflammatory processes may be a driving force of the pathology associated with AD" (Wyss-Coray, 2006). As such, neuroprotective strategies targeted at reducing microglial activity may be beneficial not only in AD dementia, but also in prodromal AD. If microglial activation is a causative factor for neuronal degeneration, it could be an important target for treatment of age-related cognitive problems. Imaging of microglial activation can contribute to better understanding of the role of inflammation in AD. It might also be useful to monitor the effect of future preventive and therapeutic treatments in clinical trials.

In conclusion, small clusters of increased (*R*)-[^{11}C]PK11195 binding were found in AD patients but not in prodromal AD subjects, indicating that microglial activation is a subtle phenomenon present in AD. Imaging of microglial activation may contribute to better understanding of the role of inflammation in AD.

Disclosure statement

There are no actual or potential conflicts of interest for any of the authors.

The data contained in this manuscript have not been previously published, have not been submitted elsewhere, and will not be submitted elsewhere while under consideration at *Neurobiology of Aging*.

The study protocol was approved by the Medical Ethics Review Committee of the VU University Medical Center.

All authors have reviewed the contents of the manuscript being submitted, approve of its contents, and validate the accuracy of the data.

Acknowledgements

This project was supported in part by European Commission project NCI-MCI (QLK6-CT-2000-00502) and by the Netherlands Brain Foundation (grant number 9F01.21). The authors thank Maqsood Yaqub, Henri Greuter, and Mark Lubberink for assistance and useful comments.

References

Akiyama, H., Barger, S., Barnum, S., Bradt, B., Bauer, J., Cole, G.M., Cooper, N.R., Eikelenboom, P., Emmerling, M., Fiebich, B.L., Finch, C.E., Frautschy, S., Griffin, W.S., Hampel, H., Hull, M., Landreth, G., Lue, L., Mrak, R., Mackenzie, I.R., McGeer, P.L., O'Banion, M.K., Pachter, J., Pasinetti, G., Plata-Salaman, C., Rogers, J., Rydel, R., Shen, Y., Streit, W., Strohmeyer, R., Tooyoma, I., Van Muiswinkel, F.L., Veerhuis, R., Walker, D., Webster, S., Wegrzyniak, B., Wenk, G., Wyss-Coray, T., 2000. Inflammation and Alzheimer's disease. Neurobiol. Aging 21, 383–421.

American Psychiatric Association, 2000. Diagnostic and Statistical Manual of Mental Disorders. 4th edition, text revision. American Psychiatric Association, Washington, DC.

Arends, Y.M., Duyckaerts, C., Rozemuller, J.M., Eikelenboom, P., Hauw, J.J., 2000. Microglia, amyloid and dementia in Alzheimer disease. A correlative study. Neurobiol. Aging 21, 39–47.

Boellaard, R., Turkheimer, F., Hinz, R., Schuitemaker, A., Scheltens, P., van Berckel, B.N., Lammertsma, A.A., 2008. Performance of a modified supervised cluster algorithm for extracting reference tissue input functions from (R)-[11C]PK11195 PET studies. IEEE Medical Imaging Conference Program 209 (M10-504).

Bouwman, F.H., Verwey, N.A., Klein, M., Kok, A., Blankenstein, M.A., Sluimer, J.D., Barkhof, F., van der Flier, W.M., Scheltens, P., 2010. New research criteria for the diagnosis of Alzheimer's disease applied in a memory clinic population. Dement. Geriatr. Cogn. Disord. 30, 1–7.

Braak, H., Braak, E., 1991. Neuropathological stageing of Alzheimer-related changes. Acta Neuropathol. 82, 239–259.

Brix, G., Zaers, J., Adam, L.E., Bellemann, M.E., Ostertag, H., Trojan, H., Haberkorn, U., Doll, J., Oberdorfer, F., Lorenz, W.J., 1997. Performance evaluation of a whole-body PET scanner using the NEMA protocol. National Electrical Manufacturers Association. J. Nucl. Med. 38, 1614–1623.

Cagnin, A., Brooks, D.J., Kennedy, A.M., Gunn, R.N., Myers, R., Turkheimer, F.E., Jones, T., Banati, R.B., 2001. In-vivo measurement of activated microglia in dementia. Lancet 358, 461–467.

DiPatre, P.L., Gelman, B.B., 1997. Microglial cell activation in aging and Alzheimer disease: partial linkage with neurofibrillary tangle burden in the hippocampus. J. Neuropathol. Exp. Neurol. 56, 143–149.

Dubois, B., Feldman, H.H., Jacova, C., Cummings, J.L., DeKosky, S.T., Barberger-Gateau, P., Delacourte, A., Frisoni, G., Fox, N.C., Galasko, D., Gauthier, S., Hampel, H., Jicha, G.A., Meguro, K., O'Brien, J., Pasquier, F., Robert, P., Rossor, M., Salloway, S., Sarazin, M., de Souza, L.C., Stern, Y., Visser, P.J., Scheltens, P., 2010. Revising the definition of Alzheimer's disease: a new lexicon. Lancet Neurol. 9, 1118–1127.

Edison, P., Archer, H.A., Gerhard, A., Hinz, R., Pavese, N., Turkheimer, F.E., Hammers, A., Tai, Y.F., Fox, N., Kennedy, A., Rossor, M., Brooks, D.J., 2008. Microglia, amyloid, and cognition in Alzheimer's disease: an [^{11}C](*R*)PK11195-PET and [^{11}C]PIB-PET study. Neurobiol. Dis. 32, 412–419.

Folstein, M.F., Folstein, S.E., McHugh, P.R., 1975. "Mini-mental state". A practical method for grading the cognitive state of patients for the clinician. J. Psychiatr. Res. 12, 189–198.

Genovese, C.R., Lazar, N.A., Nichols, T., 2002. Thresholding of statistical maps in functional neuroimaging using the false discovery rate. Neuroimage 15, 870–878.

Gunn, R.N., Lammertsma, A.A., Hume, S.P., Cunningham, V.J., 1997. Parametric imaging of ligand-receptor binding in PET using a simplified reference region model. Neuroimage 6, 279–287.

Hoekstra, C.J., Paglianiti, I., Hoekstra, O.S., Smit, E.F., Postmus, P.E., Teule, G.J., Lammertsma, A.A., 2000. Monitoring response to therapy in cancer using [^{18}F]-2-fluoro-2-deoxy-D-glucose and positron emission tomography: an overview of different analytical methods. Eur. J. Nucl. Med. 27, 731–743.

Hoozemans, J.J., van Haastert, E.S., Veerhuis, R., Arendt, T., Scheper, W., Eikelenboom, P., Rozemuller, A.J., 2005. Maximal COX-2 and ppRb expression in neurons occurs during early Braak stages prior to the maximal activation of astrocytes and microglia in Alzheimer's disease. J. Neuroinflammation 2, 27.

Hudson, H.M., Larkin, R.S., 1994. Accelerated image reconstruction using ordered subsets of projection data. IEEE Trans. Med. Imaging 13, 601–609.

Innis, R.B., Cunningham, V.J., Delforge, J., Fujita, M., Gjedde, A., Gunn, R.N., Holden, J., Houle, S., Huang, S.C., Ichise, M., Iida, H., Ito, H., Kimura, Y., Koeppe, R.A., Knudsen, G.M., Knuuti, J., Lammertsma, A.A., Laruelle, M., Logan, J., Maguire, R.P., Mintun, M.A., Morris, E.D., Parsey, R., Price, J.C., Slifstein, M., Sossi, V., Suhara, T., Votaw, J.R., Wong, D.F., Carson, R.E., 2007. Consensus nomenclature for in vivo imaging of reversibly binding radioligands. J. Cereb. Blood Flow Metab. 27, 1533–1539.

Lammertsma, A.A., Hume, S.P., 1996. Simplified reference tissue model for PET receptor studies. Neuroimage 4, 153–158.

Logan, J., Fowler, J.S., Volkow, N.D., Wang, G.J., Ding, Y.S., Alexoff, D.L., 1996. Distribution volume ratios without blood sampling from graphical analysis of PET data. J. Cereb. Blood Flow Metab. 16, 834–840.

Logan, J., Fowler, J.S., Volkow, N.D., Wolf, A.P., Dewey, S.L., Schlyer, D.J., MacGregor, R.R., Hitzemann, R., Bendriem, B., Gatley, S.J., 1990. Graphical analysis of reversible radioligand binding from time-activity measurements applied to [N-11C-methyl]-(–)-cocaine PET studies in human subjects. J. Cereb. Blood Flow Metab. 10, 740–747.

Maes, F., Collignon, A., Vandermeulen, D., Marchal, G., Suetens, P., 1997. Multimodality image registration by maximization of mutual information. IEEE Trans. Med. Imaging 16, 187–198.

McKhann, G., Drachman, D., Folstein, M., Katzman, R., Price, D., Stadlan, E.M., 1984. Clinical diagnosis of Alzheimer's disease: report of the NINCDS-ADRDA Work Group under the auspices of Department of Health and Human Services Task Force on Alzheimer's Disease. Neurology 34, 939–944.

Meyer-Luehmann, M., Spires-Jones, T.L., Prada, C., Garcia-Alloza, M., de Calignon, A., Rozkalne, A., Koenigsknecht-Talboo, J., Holtzman, D.M., Bacskai, B.J., Hyman, B.T., 2008. Rapid appearance and local toxicity of amyloid-beta plaques in a mouse model of Alzheimer's disease. Nature 451, 720–724.

Morris, J.C., Storandt, M., Miller, J.P., McKeel, D.W., Price, J.L., Rubin, E.H., Berg, L., 2001. Mild cognitive impairment represents early-stage Alzheimer disease. Arch. Neurol. 58, 397–405.

Mourik, J.E., Lubberink, M., van Velden, F.H., Kloet, R.W., van Berckel, B.N., Lammertsma, A.A., Boellaard, R., 2010. In vivo validation of

reconstruction-based resolution recovery for human brain studies. J. Cereb. Blood Flow Metab. 30, 381–389.

Okello, A., Edison, P., Archer, H.A., Turkheimer, F.E., Kennedy, J., Bullock, R., Walker, Z., Kennedy, A., Fox, N., Rossor, M., Brooks, D.J., 2009. Microglial activation and amyloid deposition in mild cognitive impairment: a PET study. Neurology 72, 56–62.

Ollinger, J.M., Fessler, J.A., 1997. Positron Emission Tomography, IEEE Signal Processing Magazine 14. 1st edition, pp 43–55.

Papadopoulos, V., Baraldi, M., Guilarte, T.R., Knudsen, T.B., Lacapère, J.J., Lindemann, P., Norenberg, M.D., Nutt, D., Weizman, A., Zhang, M.R., Gavish, M., 2006. Translocator protein (18kDa): new nomenclature for the peripheral-type benzodiazepine receptor based on its structure and molecular function. Trends Pharmacol. Sci. 27, 402–409.

Petersen, R.C., 2004. Mild cognitive impairment as a diagnostic entity. J. Intern. Med. 256, 183–194.

Petersen, R.C., Parisi, J.E., Dickson, D.W., Johnson, K.A., Knopman, D.S., Boeve, B.F., Jicha, G.A., Ivnik, R.J., Smith, G.E., Tangalos, E.G., Braak, H., Kokmen, E., 2006. Neuropathologic features of amnestic mild cognitive impairment. Arch. Neurol. 63, 665–672.

Petersen, R.C., Smith, G.E., Waring, S.C., Ivnik, R.J., Tangalos, E.G., Kokmen, E., 1999. Mild cognitive impairment: clinical characterization and outcome. Arch. Neurol. 56, 303–308.

Price, J.L., Morris, J.C., 1999. Tangles and plaques in nondemented aging and "preclinical" Alzheimer's disease. Ann. Neurol. 45, 358–368.

Rozemuller, J.M., Eikelenboom, P., Pals, S.T., Stam, F.C., 1989. Microglial cells around amyloid plaques in Alzheimer's disease express leucocyte adhesion molecules of the LFA-1 family. Neurosci. Lett. 101, 288–292.

Schuitemaker, A., van Berckel, B.N., Kropholler, M.A., Kloet, R.W., Jonker, C., Scheltens, P., Lammertsma, A.A., Boellaard, R., 2007a. Evaluation of methods for generating parametric (*R*)-[^{11}C]PK11195 binding images. J. Cereb. Blood Flow Metab. 27, 1603–1615.

Schuitemaker, A., van Berckel, B.N., Kropholler, M.A., Veltman, D.J., Scheltens, P., Jonker, C., Lammertsma, A.A., Boellaard, R., 2007b. SPM analysis of parametric (*R*)-[^{11}C]PK11195 binding images: plasma input versus reference tissue parametric methods. Neuroimage 35, 1473–1479.

Schuitemaker, A., van der Doef, T.F., Boellaard, R., van der Flier, W.M., Yaqub, M., Windhorst, A.D., Barkhof, F., Jonker, C., Kloet, R.W., Lammertsma, A.A., Scheltens, P., van Berckel, B.N., 2012. Microglial activation in healthy aging. Neurobiol. Aging 33, 1067–1072.

Shah, F., Hume, S.P., Pike, V.W., Ashworth, S., McDermott, J., 1994. Synthesis of the enantiomers of [N-methyl-^{11}C]PK 11195 and comparison of their behaviours as radioligands for PK binding sites in rats. Nucl. Med. Biol. 21, 573–581.

Svarer, C., Madsen, K., Hasselbalch, S.G., Pinborg, L.H., Haugbøl, S., Frøkjaer, V.G., Holm, S., Paulson, O.B., Knudsen, G.M., 2005. MR-based automatic delineation of volumes of interest in human brain PET images using probability maps. Neuroimage 24, 969–979.

Turkheimer, F.E., Edison, P., Pavese, N., Roncaroli, F., Anderson, A.N., Hammers, A., Gerhard, A., Hinz, R., Tai, Y.F., Brooks, D.J., 2007. Reference and target region modeling of [^{11}C]-(R)-PK11195 brain studies. J. Nucl. Med. 48, 158–167.

Veerhuis, R., Van Breemen, M.J., Hoozemans, J.M., Morbin, M., Ouladhadj, J., Tagliavini, F., Eikelenboom, P., 2003. Amyloid beta plaque-associated proteins C1q and SAP enhance the Abeta1-42 peptide-induced cytokine secretion by adult human microglia in vitro. Acta Neuropathol. 105, 135–144.

Venneti, S., Lopresti, B.J., Wiley, C.A., 2006. The peripheral benzodiazepine receptor (Translocator protein 18kDa) in microglia: from pathology to imaging. Prog. Neurobiol. 80, 308–322.

West, J., Fitzpatrick, J.M., Wang, M.Y., Dawant, B.M., Maurer, C.R., Jr, Kessler, R.M., Maciunas, R.J., Barillot, C., Lemoine, D., Collignon, A., Maes, F., Suetens, P., Vandermeulen, D., van den Elsen, P.A., Napel, S., Sumanaweera, T.S., Harkness, B., Hemler, P.F., Hill, D.L., Hawkes, D.J., Studholme, C., Maintz, J.B., Viergever, M.A., Malandain, G., Woods, R.P., 1997. Comparison and evaluation of retrospective intermodality brain image registration techniques. J. Comput. Assist. Tomogr. 21, 554–566.

Wiley, C.A., Lopresti, B.J., Venneti, S., Price, J., Klunk, W.E., DeKosky, S.T., Mathis, C.A., 2009. Carbon 11-labeled Pittsburgh compound B and carbon 11-labeled (R)-PK11195 positron emission tomographic imaging in Alzheimer disease. Arch. Neurol. 66, 60–67.

Wyss-Coray, T., 2006. Inflammation in Alzheimer disease: driving force, bystander or beneficial response? Nat. Med. 12, 1005–1015.

Yaqub, M., Van Berckel, B.N.M., Schuitemaker, A., Hinz, R., Turkheimer, F., Lammertsma, A.A., Boellaard, R., 2009. Optimisation of Supervised Cluster Analysis for Extracting Reference Tissue Input Curves in (R)-[^{11}C]PK11195 Studies. J. Cereb. Blood Flow Metab. 29 pp. S1–S5.

Yokokura, M., Mori, N., Yagi, S., Yoshikawa, E., Kikuchi, M., Yoshihara, Y., Wakuda, T., Sugihara, G., Takebayashi, K., Suda, S., Iwata, Y., Ueki, T., Tsuchiya, K.J., Suzuki, K., Nakamura, K., Ouchi, Y., 2011. In vivo changes in microglial activation and amyloid deposits in brain regions with hypometabolism in Alzheimer's disease. Eur. J. Nucl. Med. Mol. Imaging 38, 343–351.

Yoshiyama, Y., Higuchi, M., Zhang, B., Huang, S.M., Iwata, N., Saido, T.C., Maeda, J., Suhara, T., Trojanowski, J.Q., Lee, V.M., 2007. Synapse loss and microglial activation precede tangles in a P301S tauopathy mouse model. Neuron 53, 337–351.